We are IntechOpen, the world's leading publisher of Open Access books Built by scientists, for scientists

4,800
Open access books available

122,000
International authors and editors

135M
Downloads

Our authors are among the

154
Countries delivered to

TOP 1%
most cited scientists

12.2%
Contributors from top 500 universities

WEB OF SCIENCE™

Selection of our books indexed in the Book Citation Index in Web of Science™ Core Collection (BKCI)

Interested in publishing with us?
Contact book.department@intechopen.com

Numbers displayed above are based on latest data collected.
For more information visit www.intechopen.com

13

Dynamics of Optical Pulses Propagating in Fibers with Variable Dispersion

Alexej A. Sysoliatin[1], Andrey I. Konyukhov[2] and Leonid A. Melnikov[3]
[1]*Fiber Optics Research Center, Vavilov Street 38, Moscow*
[2]*Saratov State University, Astrakhanskaya 83, Saratov*
[3] *Saratov State Technical University, Politehnicheskaya 77, Saratov*
Russia

1. Introduction

The book chapter describes recent progress in the management of laser pulses by means of optical fibers with smoothly variable dispersion. Nonlinear Schrödinger equation based numerical simulations give powerful mathematics for optimizing of fiber dispersion for given task. In the book chapter we use numerical simulations to describe and analyse soliton and pulse dynamics in three kind of fibers with variable dispersion: i) dispersion oscillating fiber; ii) negative dispersion decreasing fiber. Optical pulse compression techniques are important for the generation of subpicosecond and femtosecond optical pulses. Dispersion decreasing fibers are useful for high quality, pedestal-free optical pulse compression.

The classical soliton concept was developed for nonlinear and dispersive systems that have been autonomous; namely, propagation distance has only played the role of the independent variable and has not appeared explicitly in the nonlinear Schrödinger equation (NLSE) (Ablowitz et al., 1981; Agraval, 2001; Akhmanov et al., 1991). Under condition of harmonical dispersion and nonlinearity nonautonomous solitons interact elastically and generally move with varying amplitudes, speeds, and spectra (Serkin et al., 2007).

High-order soliton propagating in a fiber with fixed dispersion and nonlinearity is reshaped periodically after propagation distance equal to the soliton period $0.16\pi|\beta_2|^{-1}T_{\mathrm{FWHM}}^2$ (Agraval, 2001; Akhmanov et al., 1991), where β_2 is second order dispersion coefficient, T_{FWHM} is the full-width at half-maximum (FWHM) pulse duration. In a fiber with periodically modulated core diameter, the dispersion oscillates periodically along the fiber length. When the oscillation period approaches the soliton period, the soliton splits into few pulses. Simulations show that second-order soliton splits into two pulses, which carrier frequencies are located symmetrically with respect to the initial pulse frequency (Bauer et al., 1995; Hasegava et al., 1991). A sequence of second-order solitons transmitted through dispersion oscillating fiber (DOF) will produce a pulse train with alternate carrier frequency.

Nonlinear pulse propagation in periodic transmission lines with multisegmented fibers was investigated extensively. The dispersion managed soliton (Malomed, 2006; Smith et al., 1996), split-step soliton (Driben et al., 2000), and stationary rescaled pulse (Inoue et al., 2005) have been discovered. The studies were focused mainly on the stability of solitons.

Simulations show that soliton splitting into the pairs of pulses with upshifted and downshifted central wavelengths can be achieved by a stepwise change of dispersion or by a localized loss element or filter (Lee et al., 2003). The maximum spectral separation occurs at locations that correspond to a half of soliton period for second-order soliton and to 0.225 of soliton period for third-order soliton. In a fiber that consists of a few segments, the multiple breakups of each soliton can generate Cantor set fractals (Sears et al., 2000). Theoretical studies (Bauer et al., 1995; Hasegava et al., 1991; Lee et al., 2003; Sears et al., 2000) consider the soliton splitting without effect of stimulated Raman scattering or high-order dispersion. The fission of high-order soliton can be stimulated by self-steepening (Golovchenko et al., 1985), Raman scattering (Dianov et al., 1985; Tai et al., 1988), and cubic dispersion (Wai et al., 1986). These effects are not negligible for few-picosecond pulses.

Splicing losses and transient processes that arise due to a stepwise change of the dispersion restrict the application of multisegmented fibers for soliton splitting. These disadvantages of multisegmented fibers are surmountable in a fiber with a smooth modulation of the core diameter. We considered the soliton splitting in a fiber with a sine-wave variation of the fiber diameter (DOF).

Optical pulse compression techniques are important for the generation of sub-ps and fs optical pulses. Dispersion decreasing fibers (DDF) are useful for high-quality, pedestal-free optical pulse compression. There are several techniques to compress optical pulses, in particular it is possible to utilize soliton effects. Earlier research focused on using the compression of high-order solitons. This can provide rapid compression but suffers from residual pedestal. Furthermore, the pulse quality at the optimum point of compression is poor, since a significant proportion of the pulse energy is contained in a broad pedestal. A less rapid technique but with better pulse quality is adiabatic amplification of fundamental solitons. To avoid pulse distortion the amplification per soliton period cannot be too big. The method to vary dispersion along the fiber length can be used to obtain the same effect as adiabatic amplification, but the effect can be achieved in a passive fiber.

High pulse quality with minimal or no pedestal component can be achieved by the adiabatic compression technique using dispersion decreasing fibers. Improved quality pulse compression is possible and the input power requirements are significantly lower than that for soliton-effect compression. For a DDF with length L the ratio of input to output dispersion determines the maximum pulse compression factor for the case of no fiber loss and a constant nonlinearity coefficient:

$$W_{eff} = \frac{\beta_2(0)}{\beta_2(L)} \tag{1}$$

The maximum compression factor is determined by the ratio of input to output dispersion and could be over 50. Using DDF with optimum dispersion profile it is possible to obtain pedestal-free pulses of less than 200 fs duration using technique of adiabatic soliton compression (Pelusi et al., 1997). In the case of short (< 3 ps) solitons it is necessary to take into account the higher-order nonlinear and dispersive effects. In particular intrapulse Raman scattering results to the shift of the soliton mean frequency. This frequency shift leads to the change in GVD due to third-order dispersion β_3. These effects result to the soliton corruption. However the stable compression of ultrashort solitons in DDF can take place in the presence of the Raman effect and third order dispersion. Taking these effects into account it is possible to generate high quality pulses of 30 fs duration.

A tunable source can be based on the supercontinuum generation (Haus et al., 2000) and on the Raman conversion of the carrier frequency of the optical soliton (Dianov et al., 1985). Last method could be high efficient especially whether smooth tuning in some frequency range is required. Recently an efficient optical scheme has been proposed capable to generate 30 fs pulses at MHz pulse repetition rates, smoothly tuned in the telecommunication range using a high nonlinear dispersion decreasing fiber (Andrianov et al., 2007). The smooth tuning is based on the Raman frequency conversion of ultrashort pulses. However, until now nobody was able to build up the L-band tunable GHz ps source well synchronized with basic clock.
A high-repetition-rate broadband source is attractive both for high-capacity fiber transmission systems and in optical spectroscopy and metrology. The task to generate the broadband spectra in the nearby region of 1550 nm window was of remarkable interest from 1990 and since then the essential research efforts have been carried out in this area. Dense wavelength-division multiplexing is an efficient and practical method to increase the capacity of lightwave transmission systems. As the number of channels increases for such systems, the required number of lasers becomes large if each channel has its own transmitter. Under these conditions spectral slicing of a single coherent broadband transmitter has attracted attention, especially for gigabit-per-second systems in which external modulators are used. So far, spectral slicing has been limited to laboratory trials. However, the fiber transmission window has been expanded to 400 nm with the removal of the water absorption peak.
Spectral slicing may then become attractive in real systems, especially if a single source can cover the entire fiber transmission window (1300–1700 nm). Thus, a gigahertz-repetition-rate (rep-rate) broadband source can be important for high-capacity light-wave transmission systems. To achieve such a source a high-rep-rate mode-locked laser is used either as the seed for further external spectrum generation or as the source itself. Actively mode-locked lasers can provide high-rep-rate, good noise performance and can easily be locked to external clocks through their intracavity modulator. However, even with soliton pulse shortening these lasers produce only picosecond pulses. Further spectral broadening with these lasers has resulted only in limited spectral widths, even in the supercontinuum regime. Passively mode-locked lasers can provide short pulses directly and a very large externally generated bandwidth but at a low rep rate. Although passive harmonic mode locking or external time-division multiplexing can increase the rep rate of such lasers, they require extensive stabilization and (or) suffer from poor timing jitter and poor supermode suppression.

2. Pulse propagation in single mode fibers

This section covers some fundamental concepts for modelling of pulse propagation in fibers. The section describes numerical approaches used for modelling of the pulse propagation in single-mode fibers with variable dispersion. For this aim nonlinear Schrödinger equation (NLS) (or complex Ginzburg-Landau equation) is used. Split-step method with time-frequency Fourier transform is applied for solving the NLS equation. We examine the method of inverse scattering transform in application to numerical analysis of solitons dynamics in presence of variable dispersion, pulse self-steepening and stimulated Raman scattering. Numerical approaches used for solving and analysis of NLS equation are described in sections below.

2.1 Propagation equation

We assume that the incident light is polarized along a principal axis (for example chosen to coincide with the x axis). In time-domain the pulsed optical field can be presented as superposition of monochromatic waves

$$E_t(r,\phi,z) = \int_{-\infty}^{\infty} d\omega \mathcal{A}_\omega \psi(r,\phi,\omega) \exp\left[-i\omega t + i\beta(\omega)z\right] + \text{c.c.} \simeq$$

$$\psi(r,\phi,\omega_0) \int_{-\infty}^{\infty} d\omega \mathcal{A}_\omega \exp\left[-i\omega t + i\beta(\omega)z\right] + \text{c.c.}, \tag{2}$$

where ω is the field frequency, (r,ϕ) are transverse coordinates, z is the propagation distance, $A(\omega)$ is the mode amplitude, $\beta(\omega)$ is called propagation constant which is z-component of wavevector, "c.c." is complex conjugate, $\psi(r,\phi,\omega)$ describes transverse distribution of the mode field. The optical field is assumed to be quasi-monochromatic, i.e., the pulse spectrum, centered at ω_0, is assumed to have a spectral width $\Delta\omega \ll 1$. Thus the frequency dependence of ψ in (2) can be neglected and $\psi(r,\phi,\omega) \simeq \psi(r,\phi,\omega_0)$ where ω_0 is the pulse central frequency For weakly guiding step-profile fiber the function $\psi(r,\phi)$ gives transverse field distribution for LP_{01} mode (see section 12-11 in (Snyder et al., 1983))

$$\psi(r,\phi) = \begin{cases} \frac{J_0(ur/a)}{J_0(u)}, & r \le a, \\ \frac{K_0(wr/a)}{K_0(w)}, & r > a \end{cases}, \tag{3}$$

where J_0 and J_1 are Bessel functions of the first kind, K_0 and K_1 are modified Bessel functions of the second kind, a is fiber core radius. Frequency dependent functions $u(\omega)$, $w(\omega)$ are defined from eigenvalue equation

$$u\frac{J_1(u)}{J_0(u)} = w\frac{K_1(w)}{K_0(w)}, \tag{4}$$

where $u^2 + w^2 = V^2$. Propagation constant can be found as $\beta^2 = k^2 n_c^2 - u^2/a^2$, where $k = \omega/c$ is wavenumber, n_c is the fiber core refractive index.

For optical fibers having complex transverse distribution of refractive index the propagation constant $\beta(\omega)$ can be calculated numerically. Different methods for Bragg fibers (Yeh et al., 1978),(Guo et al., 2004), photonic crystal fibers and microstructure fibers (Poli et al., 2007), (Lourtioz et al., 2005), (Brechet et al., 2000) are proposed.

Equation (2) is inverse Fourier transform. At $z = 0$ integral (2) gives Fourier transformation of input pulse $E_t(r,\phi,z) = \psi(r,\phi,\omega_0)A(t)$, where slowly varying pulse amplitude

$$A(t) = \int_{-\infty}^{\infty} d\omega \mathcal{A}_\omega e^{-i\omega t}, \tag{5}$$

$$\mathcal{A}_\omega = \frac{1}{2\pi} \int_{-\infty}^{\infty} dt A(t) e^{i\omega t}. \tag{6}$$

$$\mathcal{E}_\omega(r,\phi,z) = \mathcal{A}_\omega \psi(r,\phi,\omega_0) \exp\left[-i\omega_0 t + i\beta(\omega)z\right] + \text{c.c.}, \tag{7}$$

Taylor series of $\beta(\omega)$ about the central pulse frequency ω_0 is

$$\beta(\omega) = \beta(\omega_0) + \frac{1}{v_g}\Omega + \frac{\beta_2}{2}\Omega^2 + \sum_{m=3}\frac{\beta_m}{m!}\Omega^m \tag{8}$$

where v_g is the group velocity, $\Omega = \omega - \omega_0$

$$\frac{1}{v_g} = \frac{d\beta}{d\omega}\Big|_{\omega=\omega_0}, \qquad \beta_m = \frac{d^m\beta}{d\omega^m}\Big|_{\omega=\omega_0}. \tag{9}$$

Parameter β_2 represents dispersion of the group velocity and is responsible for pulse broadening. This phenomenon is known as the group-velocity dispersion (GVD), and β_2 is the GVD parameter (Agraval, 2001). For modelling femtosecond pulse propagation in microstructure fiber up to six-order dispersion coefficients can be used (Washburn et al., 2002). With large number terms ($m > 10$) the Taylor series (8) roughly approximate dispersion due to computing errors grows.

Pulse propagation in single mode fibers described by so-called generalized nonlinear Schrödinger equation (NLS) or generalized complex Ginzburg-Landau equation. Detailed derivation of this equation can be found in literature (Agraval, 2001), (Akhmanov et al., 1991), (Kivshar et al., 2003). Including high-order dispersion terms β_m the NLS equation takes form

$$\frac{\partial A}{\partial z} + \frac{\alpha}{2} + i\frac{\beta_2}{2}\frac{\partial^2 A}{\partial \tau^2} - i\sum_{m=3} i^m \frac{\beta_m}{m!}\frac{\partial^m A}{\partial \tau^m} = i\left(P_{NL} + i\frac{2}{\omega_0}\frac{\partial P_{NL}}{\partial \tau}\right). \tag{10}$$

where $\tau = t - z/v_g$ is the local time in coordinate system moving with the pulse at the group velocity v_g, α describes the effects of fiber losses, P_{NL} is nonlinear media polarization

$$P_{NL}(z,\tau) = \gamma|A|^2 A + \gamma_R Q(z,\tau)A(z,\tau). \tag{11}$$

The media polarization P_{NL} includes both the electronic and vibrational (Raman) contributions. The term $\gamma|A|^2A$ describes instantaneous Kerr nonlinearity, $\gamma_R Q(z,t)A(z,t)$ associated with stimulated Raman scattering. The time derivative appearing on the right-hand side of Eq. (10) is responsible for self-steepening and shock formation (Akhmanov et al., 1991) at a pulse edge.

Nonlinear parameter γ in eq. (11) is defined as

$$\gamma = \frac{\omega_0 n_2}{cA_{\text{eff}}}, \tag{12}$$

In scalar approach the effective area is

$$A_{\text{eff}} = \frac{\left(\int_0^{2\pi}\int_0^{\infty}|\psi(r,\phi)|^2 r dr d\phi\right)^2}{\int_0^{2\pi}\int_0^{\infty}|\psi(r,\phi)|^4 r dr d\phi}, \tag{13}$$

In (Lægsgaard et al., 2003) modified formula for effective area is proposed

$$A_{\text{eff}} = \left(\frac{n_1}{n_0^g}\right)^2 \frac{\left(\int (\vec{E}\cdot\vec{D})rdrd\phi\right)^2}{\int_{\text{SiO}_2} |\vec{E}\cdot\vec{D}|^2 rdrd\phi}, \tag{14}$$

where $\vec{D}$ is electric flux density of fundamental mode, n_0^g is effective group index of the mode, n_1 is the refractive index of silica in the limit of zero field. Note that the integration in the denominator is restricted to the silica parts fiber that contains air holes running along its length. Eq. (14) was applied for calculating of effective mode area in silica-based photonic bandgap fibers (Lægsgaard et al., 2003). This formula has been derived without making assumptions about the field energy distribution and is therefore applicable even in the case conventional fibers that guide light in silica or other materials.

Considering a mean value of the Raman gain efficiency $\bar{g}_R$ in the fiber cross-section, the relation between the Raman gain coefficient and the Raman effective area can be expressed as $\gamma_R = \bar{g}_R / A_{\text{eff}}^R$ (see for example Chapter 5 in (Poli et al., 2007)). Nonlinear parameter γ_R is responsible for Raman gain in (11). Notice that the coefficient $\bar{g}_R$ represents a total value of the Raman gain efficiency associated with the fiber, which takes into account the materials that compose the fiber and their spatial distribution. If the interacting signals have the same frequency, the Raman effective area coincides with that given by the "classical" definition (13).

Nonlinear susceptibility $Q(z,\tau)$ in equation (11) for media polarization can be expressed as convolution

$$Q(z,\tau) = \int_{-\infty}^{\infty} h_R(t')|A(z,\tau-t')|^2 dt', \tag{15}$$

where

$$h_R(\tau) = \frac{T_1^2+T_2^2}{T_1 T_2^2} \exp(-\tau/T_2)\sin(\tau/T_1). \tag{16}$$

Parameters T_1 and T_2 are two adjustable parameters and are chosen to provide a good fit to the actual Raman-gain spectrum. Their appropriate values are T_1=12.2 fs and T_2=32 fs. The Fourier transform $\tilde{h}_R(\omega)$ of $h_R(\tau)$ can be written as

$$\tilde{h}_R(\omega) = \frac{T_1^2+T_2^2}{T_2^2+T_1^2(1-i\omega T_2^2)^2}. \tag{17}$$

Using Fourier transform $\mathcal{F}(|A(z,\tau)|^2)$ at the given plane z the function $Q(z,\tau)$ can be calculated as

$$Q(z,\tau) = \mathcal{F}^{-1}\left[\tilde{h}_R(\omega)\cdot\mathcal{F}(|A(z,\tau)|^2)\right], \tag{18}$$

where $\mathcal{F}^{-1}$ denote inverse Fourier transform.

Another approach for description of Raman delayed response is based on the approximation of $Q(z,\tau)$ by damping oscillations (Belenov et al., 1992):

$$\frac{\partial^2 Q}{\partial t^2} + \frac{2}{T_2}\frac{\partial Q}{\partial t} + \frac{1}{T_1^2}Q(z,t) = \frac{1}{T_1^2}|A(z,t)|^2. \tag{19}$$

Under assumption $T_1 \ll T_2$ eq. (19) can be reduced to eq.(15). Calculation of $Q(\tau)$ for the given $A(z,\tau)$ at the fixed plane z can be done by finite-difference scheme for (19). Such scheme can be somewhat convenient than inverse Fourier transform (18).

2.2 Numerical methods

For modelling of the pulse propagation in single mode fiber split-step Fourier method was applied (Agraval, 2001), (Malomed, 2006). Figure 1 shows numerical scheme applied for single propagation step Δz. Functions $Q(\tau)$ and $\partial P_{NL}/\partial\tau$ are calculated under a periodic boundary condition that imposed upon discrete Fourier transform. Use of periodic boundary condition for the given temporal frame allows to simulate the propagation of pulse train generated by a modelocked laser. For picosecond pulses which central frequency ω_0 is far from zero of the group velocity dispersion two dispersion terms β_2 and β_3 are sufficient. For z-dependent dispersion and nonlinearity coefficients $\beta_m(z)$, $\gamma(z)$ and $\gamma_R(z)$ should be evaluated for each z. The scheme (fig. 1) is performed repeatedly until fiber end is reached.

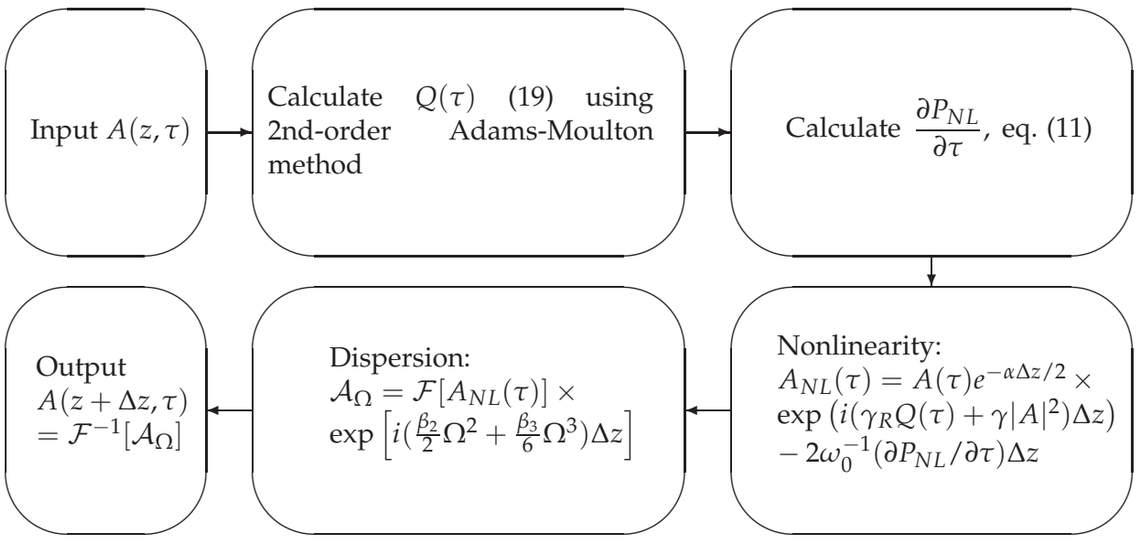

Fig. 1. Numerical scheme for the pulse propagation from plane z to the plane $z + \Delta z$. $\mathcal{F}$ is the fast forward Fourier transform (FFT), $\mathcal{F}^{-1}$ is the fast inverse Fourier transform (IFT).

2.3 Optical solitons

Optical solitons arize due to interplay between anomalous dispersion ($\beta_2 < 0$) and Kerr self-phase modulation. The solitons are solutions of nonlinear Schrödinger equation (NLS)

$$\frac{\partial A}{\partial z} + i\frac{\beta_2}{2}\frac{\partial^2 A}{\partial \tau^2} = i\gamma|A|^2 A(z,\tau). \tag{20}$$

Eq. (20) obtained from (10) neglecting by high-order dispersion terms ($\beta_m = 0$, $m = 3,4,5\ldots$), by stimulated Raman scattering ($\gamma_R = 0$) and by self-steepening ($\partial P_{NL}/\partial\tau = 0$).
NLS (20) has specific pulselike solutions that either do not change along fiber length or follow a periodic evolution pattern – such solutions are known as optical solitons. Their properties

were understood completely using inverse scattering method (Ablowitz et al., 1981). Details of the inverse scattering method in application to the optical solitons are available in literature (Agraval, 2001; Akhmanov et al., 1991; Malomed, 2006).
Initial field

$$A(0,\tau) = N\sqrt{\frac{|\beta_2|}{\gamma\tau_0}}\,\mathrm{sech}\left(\frac{\tau}{\tau_0}\right) \tag{21}$$

where τ_0 is initial pulse width. For integer N (21) give so-called N-soliton solution,
The first-order soliton $(N = 1)$ corresponds to fundamental soliton It is referred to as the fundamental soliton because its shape does not change on propagation in the fiber with fixed dispersion. In the fiber with variable dispersion nonautonomous optical solitons propagate with varying amplitudes, speeds, and spectra. Analytical solution for fundamental nonautonomous solitons in (Serkin et al., 2007) is given.
Higher-order solitons are also described by the general solution of Eq. (20)

$$A(z,\tau) = \sum_{j=1}^{N} A_j\,\mathrm{sech}\left[\frac{u_j}{2}\left(\tau - zv_j\right)\right]\exp\left[i\left(\phi_0 + \frac{v_j}{2}\tau + \frac{u_j^2 - v_j^2}{4}z\right)\right], \tag{22}$$

where $A_j = 2\tau_0(|\beta_2|/\gamma)^{1/2}Im(\lambda_j)$, $v_j = 2\tau_0^{-1}Re(\lambda_j)$, $u_j = 2\tau_0^{-1}Im(\lambda_j)$, λ_j are roots of scattering matrix element of $a(\lambda) = 0$. Parameters λ_j give solitonic spectrum. The scattering matrix is

$$M(\lambda) = \begin{pmatrix} a(\lambda) & -b^*(\lambda) \\ b(\lambda) & a^*(\lambda) \end{pmatrix} =$$

$$\lim_{\tau\to\infty}\exp\left\{i\frac{\lambda}{2}\begin{pmatrix}\tau & 0\\ 0 & -\tau\end{pmatrix}\right\}\exp\left\{i\int_{-\tau}^{\tau}\sqrt{\frac{\gamma}{|\beta_2|}}\begin{pmatrix}0 & A^*\\ A & 0\end{pmatrix}\right\}\exp\left\{i\frac{\lambda}{2}\begin{pmatrix}\tau & 0\\ 0 & -\tau\end{pmatrix}\right\} \tag{23}$$

Numerical procedure for calculating (23) is described in (Akhmanov et al., 1991). The scattering matrix is calculated as product

$$M(\lambda) = \prod_{l=1,K} M_j(\lambda) = \prod_{l=1,K}\begin{pmatrix} a_l(\lambda) & -b_l^*(\lambda) \\ b_l(\lambda) & a_l^*(\lambda) \end{pmatrix} \tag{24}$$

where $M_l(\lambda)$ is partial scattering matrix, associated with temporal step $\Delta\tau = T/K$. The local time $\tau_l = -T/2 + l\Delta\tau, l = 1,\ldots,K$, K is the total number of time points,

$$a_l(\lambda) = e^{-i\lambda\Delta\tau}\left[\cos(d_l\Delta\tau) + i\lambda\frac{\sin(d_l\Delta\tau)}{d_l}\right] \tag{25}$$

$$b_l(\lambda) = ie^{i\lambda\Delta\tau}A^*(\tau_l)\sqrt{\frac{\gamma}{|\beta_2|}}\frac{\sin(d_l\Delta\tau)}{d_l}, \tag{26}$$

where $d_l = (\lambda^2 + |A(\tau_l)|^2\gamma|\beta_2|^{-1})^{1/2}$.
This procedure can be applied to numerical solution of (20) or (10). It allows to separate out amplitudes and phases of solitons.

Physically, parameters A_j and v_j in (22) represent amplitude and frequency shift respectively. Parameter u_j determines width of soliton. For the pulse (21)

$$\lambda_j = i(j - 1/2), \qquad j = 1, N \tag{27}$$

Higher-order solitons $(N > 1)$ show periodical evolution during propagation. Pulse shape is repeated over each section of length z_0 (fig.2 a).

$$z_0 = \pi \tau_0^2 |2\beta_2|^{-1} \tag{28}$$

Figure 2 shows dynamics of second-order soliton. Note that soliton parameters $Im(\lambda)$ and $Re(\lambda)$ remain unchanged (fig.2 b).

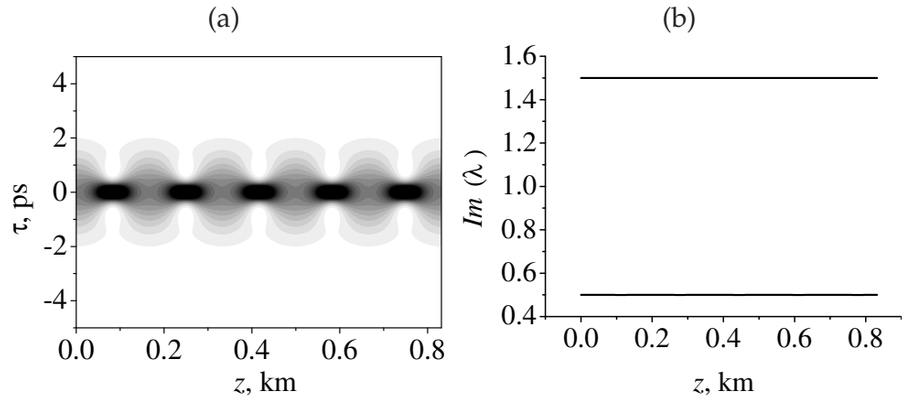

Fig. 2. Temporal evolution over five soliton periods for the second-order soliton. (a) Pulse dynamics. Black color corresponds to high intensity. (b) Soliton parameters $Im(\lambda)$. $N = 2$, $\beta_2 = -12.76\,\mathrm{ps}^2/\mathrm{km}$, $\gamma = 8.2\,\mathrm{W\ km}^{-1}$, $z_0 = 0.166$ km.

2.4 Soliton fission due to harmonic modulation of the local dispersion

In this section we consider soliton dynamics governed by nonlinear Schrödinger equation with variable second-order dispersion coefficient

$$\frac{\partial A}{\partial z} + i\frac{\beta_2(z)}{2}\frac{\partial^2 A}{\partial \tau^2} = i\gamma |A|^2 A(z,\tau). \tag{29}$$

where

$$\beta_2(z) = \langle \beta_2 \rangle \left(1 + 0.2\ \sin(2\pi\ z/z_m + \varphi_m)\right), \tag{30}$$

In the case of the harmonic periodic modulation of the local GVD coefficient, one may expect resonances between intrinsic vibrations of the free soliton. When the period of modulation of the fiber dispersion approaches the soliton period z_0, the soliton splits into pulses propagating with different group velocities (fig. 3a).

At $z = 0$ amplitudes of fundamental solitons are different $Im(\lambda_1) = 0.5$, $Im(\lambda_2) = 1.5$. But the group velocity associated with frequency shift is the same $Re(\lambda_1) = Re(\lambda_2) = 0$ (fig.3b). After single modulation period $z = z_0$ solitons acquire the same amplitudes $Im(\lambda_1) = Im(\lambda_2) = 0.987$, but different group velocities $Re(\lambda_1) = 0.411$, $Re(\lambda_2) = -0.411$. As the pulses propagates along the fiber imaginary part of λ decreases. After five modulation

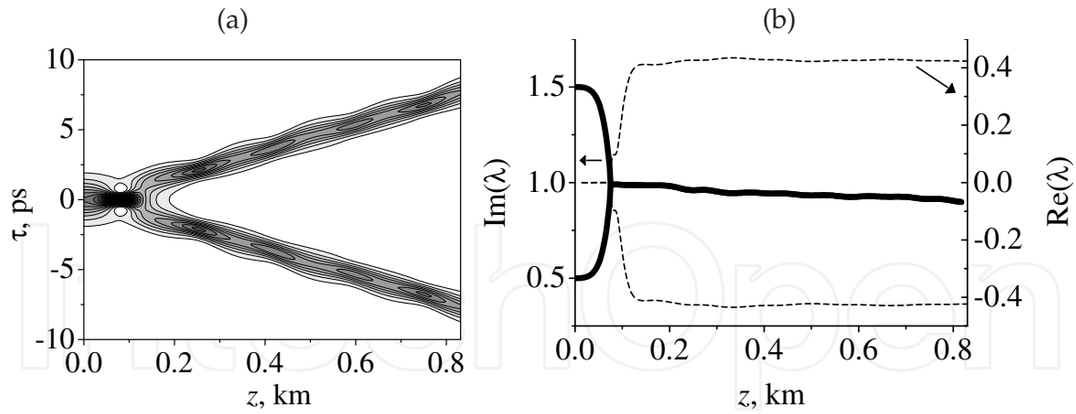

Fig. 3. A typical example of the splitting of a second-order soliton $N = 2$ into two fundamental solitons in the NLS equation with the sinusoidal modulation of the local dispersion coefficient (30). (a) Pulse dynamics; (b) $Im(\lambda)$ (solid curve, left axis) and $Im(\lambda)$ (dashed curve, right axis) $\langle\beta_2\rangle = -12.76\,\mathrm{ps}^2/\mathrm{km}$, $\varphi_m = \pi$ other parameters are the same as in Fig. 2.

periods ($z = 0.83\,\mathrm{km}$) $Im(\lambda_1) = Im(\lambda_1) = 0.89$. Decrease of $Im(\lambda(z))$ connected with emerging of dispersive wave under harmonic modulation of the group-velocity-dispersion coefficient $\beta_2(z)$.

Regime shown in fig.3 corresponds to the fundamental resonance between small vibrations of the perturbed soliton and the periodic modulation of the local GVD. Change of modulation period z_m or modulation phase φ_m can degrade the soliton split (Malomed, 2006). In the fig.4 the pulse performs a few number of irregular oscillations, but finally decay into two fundamental solitons with opposite group velocities. For $\varphi_m = 0$ (fig.4b) group velocity of output pulses is less by half than the same for $\varphi_m = \pi$ (fig.3b).

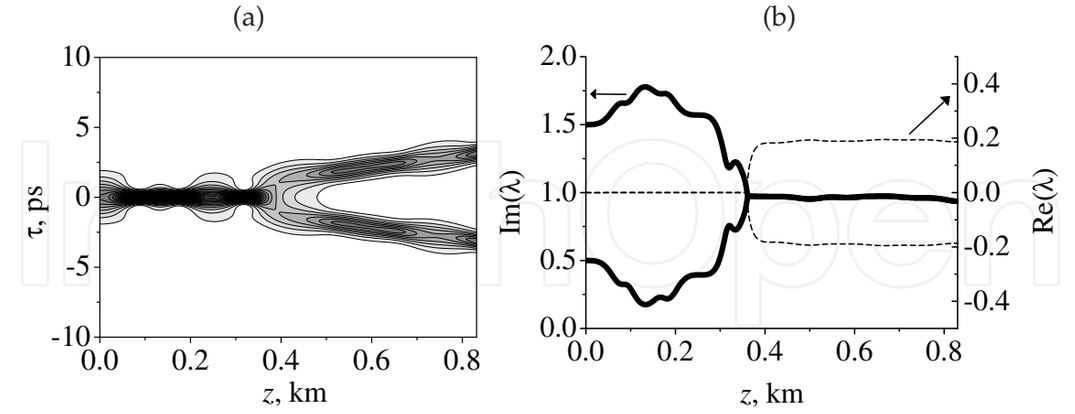

Fig. 4. Splitting of a second-order soliton into two fundamental solitons. (a) Pulse dynamics; (b) $Im(\lambda)$ (solid curve, left axis) and $Im(\lambda)$ (dashed curve, right axis) $\langle\beta_2\rangle = -12.76\,\mathrm{ps}^2/\mathrm{km}$, $z_m = z_0 = 0.166\,\mathrm{km}$, $\varphi_m = 0$ other parameters are the same as in Fig. 2.

For $\varphi_m = \pi/4$ and $N = 2$ the width of input pulse performs a large number of irregular oscillations without splitting into fundamental solitons in spite of resonant conditions $z_m = z_0 = 0.166\,\mathrm{km}$.

The parameter $N = 1.8$ corresponds to input pulse ($z = 0$) which consists of two fundamental solitons (22) having $\lambda_1 = i0.3$ and $\lambda_2 = i1.3$. The solitons remains propagating with the same group velocity (fig.5). For the constant GVD parameter $\beta_2(z) = \langle\beta_2\rangle$ the input pulse $(N = 1.8)$ performs four periods of oscillations at the propagation distance $(z = 0.83\,\text{km})$.

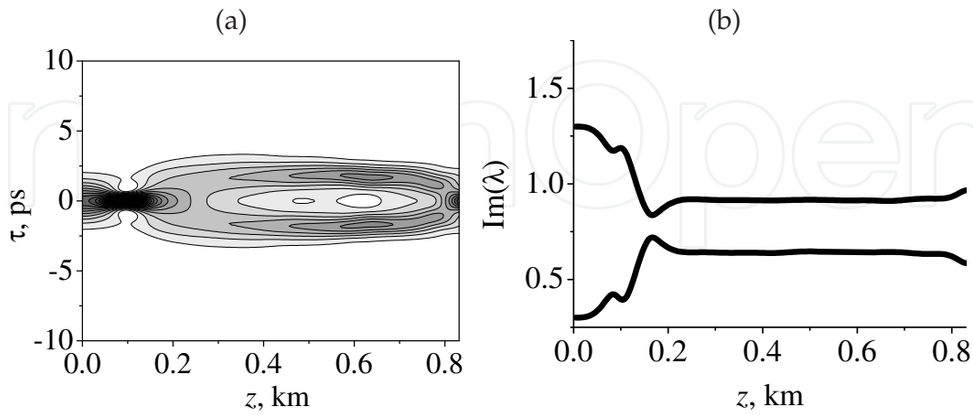

Fig. 5. Propagation of the pulse with $N = 1.8$. other parameters are the same as in Fig. 2. During propagation $Re(\lambda_1(z)) = Re(\lambda_2(z)) = 0$

3. Fission of optical solitons in dispersion oscillating fibers

Dispersion oscillating fibers have a periodic or quasi-periodic variation of the core diameter (Sysoliatin et al., 2008). Fission of second-order solitons or high-order solitons occurs due to longitudinal oscillation of the fiber dispersion and nonlinearity. In this section the results of numerical simulations of soliton fission in dispersion oscillating fiber are presented. Comparative analysis of experimental results and results of modified nonlinear Schrödinger equation based model is given. Effect of stimulated Raman scattering on the soliton fission is discussed.

3.1 Experimental confirmation

The solitons splitting described by the nonlinear Schrödinger equation with periodic perturbation was analysed in (Hasegava et al., 1991) published in 1991. However, the lack of a suitable fibers delayed experimental observation. Soliton splitting in dispersion-oscillating fiber was first observed in an experiment (Sysoliatin et al., 2008) that used a mode-locked laser (PriTel UOC) capable of emitting picosecond optical pulses near 1.55 μm, a wavelength near which optical fibers exhibit anomalous GVD together with minimum losses. Pulse repetition rate was 10 GHz. The pulses were amplified by erbium-doped fiber amplifier (EDFA) up to W =350 mW average power. The time bandwidth product for amplified pulses is found to be about $T_{\text{FWHM}}\Delta\nu = 0.304$, where $T_{\text{FWHM}} = 1.76\tau_0$ is a pulse duration and $\Delta\nu$ is the FWHM spectral pulse width. After EDFA, the pulses were launched into the DOF through fusion splicing with a single mode fiber. After propagation in 0.8-km length of DOF pulses were analyzed by intensity autocorrelator "Femtochrome" with the large scan range exceeding 100 ps and "Ando AQ6317" optical spectrum analyzer with a resolution bandwidth of 0.02 nm (fig.6).

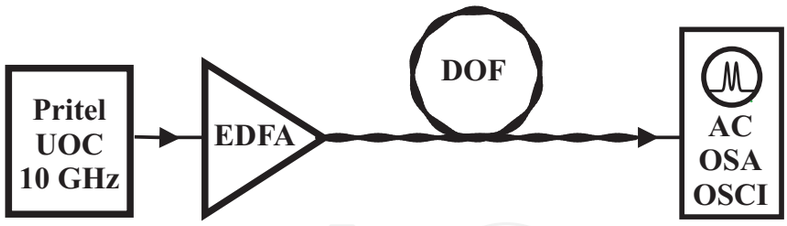

Fig. 6. Experimental setup: Pritel UOC, picosecond pulse source; EDFA, Er-doped fiber amplifier; DOF, dispersion oscillating fiber; AC, autocorrelator; OSA, optical spectrum analyzer, OSCI, wide-bandwidth oscilloscope.

The DOF was drawn in Fiber Optics Research Center (Moscow, Russia) from the preform with W-profile of refractive index. The manufactured DOF has linear loss 0.69 dB/km at 1550 nm. The fiber diameter varied slightly during the drawing in accordance with prearranged law. The variation of outer diameter of the fiber along its length is described by the sine-wave function

$$d(z) = d_0(1 + d_m \sin(2\pi z/z_m + \varphi_m)), \tag{31}$$

where $d_0 = 133\,\mu$m, $d_m = 0.03$ is the modulation depth, $z_m = 0.16$ km is the modulation period, φ_m is the modulation phase. For 0.8-km length of DOF in these experiments, $\varphi_m = 0$ at one fiber end and $\varphi_m = \pi$ at other fiber end, according to eq.(31). Thus, the modulation phase will be different for pulses launched into opposite fiber-ends.

With the average power of input pulse train below 120 mW the pulses transmitted through DOF were not split. The autocorrelation trace of output pulses have a shape typical for a train of single pulses separated by 100 ps interval. When average input power was increased, the autocorrelation trace of output pulses demonstrated three peaks (see Fig.7). Normalized intensity autocorrelation is given by:

$$C(\tau) = \left(\int |E(t)|^2 |E(t-\tau)|^2 dt\right)\left(\int |E(t)|^4 dt\right)^{-1}, \tag{32}$$

where $E(t)$ is electric field, t is the time, τ is autocorrelation delay time. Autocorrelations shown in Fig.7 correspond to two pulses $E(t) = A_1(t - T/2) + A_2(t + T/2)$ separated by temporal interval T. The value of T can be found measuring the distance between central and lateral peaks of autocorrelation function as it was shown in Fig.7(a).

The pulse splitting arises due to the fission of second order soliton. In the fiber with longitudinal variation of dispersion the second-order soliton decays into two pulses propagating with different group velocities. One of the pulses has red carrier frequency shift while the other has blue shift with respect to the initial pulse carrier frequency. The temporal separation between pulses depends on the difference between group velocities which are determined by pulse frequency shifts. In Fig.7 the pulse splitting dependence on the modulation phase and input pulse width is demonstrated. For $\varphi_m = \pi$ (Fig.7(a)(c)) the temporal interval T between pulse peaks is higher than the same for $\varphi_m = 0$ (Fig.7(b)(d)). Accordingly the largest frequency shift corresponds to the case shown in Fig.7(a)(c).

At time delay $\tau = \pm T$ the intensity autocorrelation (32) is given by

$$C(\pm T) = I_{12}/(1 + I_{12}^2), \tag{33}$$

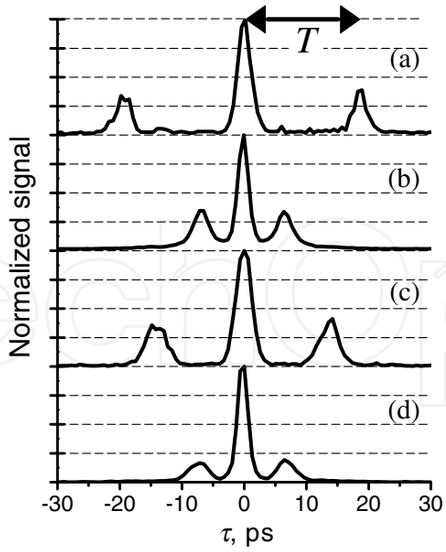

Fig. 7. Intensity autocorrelation traces of output pulses after propagation 0.8-km DOF. (a) The input average power is $P = 147.3$ mW. The input pulse width is $T_{\text{FWHM}} = 1.75$ ps. Modulation phase is $\varphi_m = \pi$. (b) $P = 150.5$ mW, $T_{\text{FWHM}} = 1.75$ ps, $\varphi_m = 0$. (c) $P = 167.4$ mW, $T_{\text{FWHM}} = 2.05$ ps, $\varphi_m = \pi$. (d) $P = 167.4$ mW, $T_{\text{FWHM}} = 2.05$ ps, $\varphi_m = 0$. The temporal interval between the peaks of output pulses T is given by the distance between peaks of autocorrelation trace as it shown in Fig.7(a).

where $I_{12} = |A_1(0)|^2/|A_2(0)|^2$ if $|A_1(0)|^2 < |A_2(0)|^2$ and $I_{12} = |A_2(0)|^2/|A_1(0)|^2$ if $|A_1(0)|^2 > |A_2(0)|^2$, $|A_1(0)|^2$ and $|A_2(0)|^2$ are peak intensities of output pulses. When the input pulse splits symmetrically ($I_{12} = 1$) the autocorrelation become $C(\pm T) = 0.5$. For autocorrelation trace shown in Fig.7(a) $C(T) = 0.38$, $C(T) = 0.33$ (Fig.7(b)), $C(T) = 0.41$ (Fig.7(c)), $C(T) = 0.19$ (Fig.7(d)). The value of $C(T)$ is underestimated due to the insufficient sensitivity of second harmonic generation (SHG) autocorrelator. However, it can be seen that for the same input power the value of $C(T)$ is higher for $\varphi_m = \pi$ (Fig.7(a)(c)) in comparison with the case $\varphi_m = 0$ (Fig.7(b)(d)). That means the case $\varphi_m = \pi$ is preferable for generation of pulse pairs with nearly identical peak intensity ($|A_1(0)|^2 \simeq |A_2(0)|^2$).
The splitting of second-order solitons produces two fundamental solitons (Bauer et al., 1995; Hasegava et al., 1991). The soliton spectrum is not broadened due to self-phase modulation because the last is balanced by negative dispersion. Spectral broadening shown in Fig.8 arises mainly due to the opposite frequency shifts of two pulses.
In time domain, the pulses are well separated (Fig.7), while in frequency domain the spectra are overlapped. Interference between these spectra leads to the modulation of the envelope of output spectrum (Fig.8(a)(b)). To a first approximation, the intensity of output spectrum can be expressed as follows:

$$\begin{aligned} F(\omega) &= |\mathcal{A}_1(\omega)e^{-i\omega(t-T/2)} + \mathcal{A}_2(\omega)e^{i\omega(t+T/2)}|^2 \\ &= |\mathcal{A}_1|^2 + |\mathcal{A}_2|^2 + 2|\mathcal{A}_1||\mathcal{A}_2|\cos[\omega T - \phi_1(\omega) + \phi_2(\omega)], \end{aligned} \tag{34}$$

where $F(\omega)$ is the spectral intensity at DOF output, $\mathcal{A}_{1,2}$ are the spectra of the first and second pulse, $\phi_{1,2} = \arg(\mathcal{A}_{1,2})$ are spectral phases. Eq. 34 shows that output spectrum is modulated

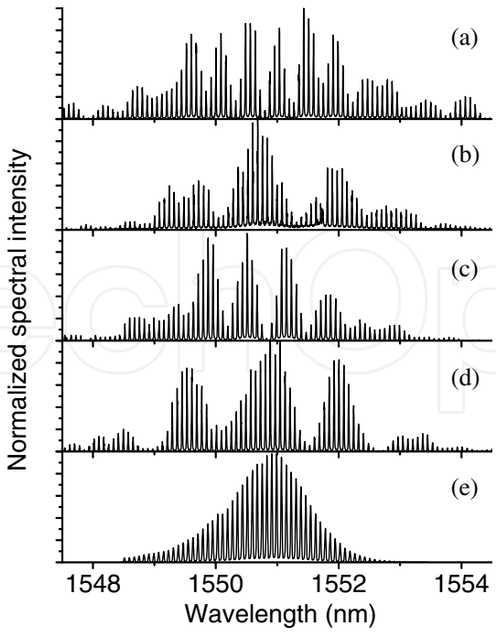

Fig. 8. Pulse train spectra. (a),(b),(c),(d) are the spectra of the output pulses, which autocorrelation traces are shown in Fig.7(a),(b),(c),(d) correspondingly. (e) the spectrum of input pulse train; FWHM spectral width of input pulses is 1.38 nm (0.172 THz).

T estimated by eq. 34	T measured
17. ps (from Fig.8(a))	18.3 ps (Fig.7(a))
6.3 ps (from Fig.8(b))	6.6 ps (Fig.7(b))
13. ps (from Fig.8(c))	14. ps (Fig.7(c))
6.3 ps (from Fig.8(d))	6.8 ps (Fig.7(d))

Table 1. Temporal interval between the peaks of output pulses.

by cosine function which period depends on the temporal interval T between two pulses. In the Table 1 the temporal interval between peaks of output pulses T is listed. The first column contains values of T estimated from spectra (Fig.8) by means of eq.(34). The second column contains the values directly measured from autocorrelation traces (Fig.7). In eq.(34) functions $\phi_{1,2}(\omega)$ are not known and assumed to be constant. This leads to underestimation of the value of T obtained from spectrum.

At large average power of input pulses train the autocorrelation trace (Fig.9(a)) and spectrum (Fig.9(b)) become more complicated. Initial pulse splits into a few low-intensity pulses and one high-intensity pulse which carrier frequency has a large red shift due to Raman scattering (Dianov et al., 1985). In Fig.9(b) the spectrum of Raman shifted pulse is located in wavelength range between 1554 nm and 1559 nm.

3.2 Modelling of soliton propagation in dispersion oscillating fibers

This section deals with solitons in the practically important model of the fibers with periodically modulated dispersion. Numerical model includes z-dependent second order and third-order dispersion coefficients $\beta_2(z)$, $\beta_3(z)$, stimulated Raman scattering and pulse self-steepening (eq. 10).

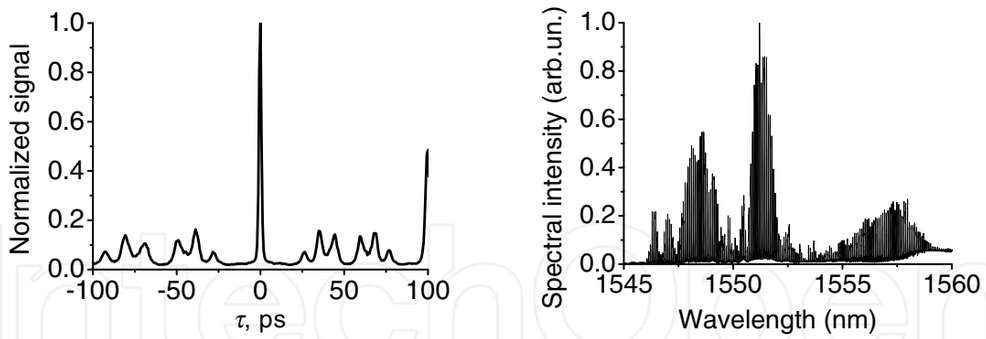

(a) (b)

Fig. 9. High power pulse transmission through DOF. (a) Autocorrelation trace. (b) pulse train spectrum. Width of initial pulse is $T_{\text{FWHM}} = 2.05\,\text{ps}$, The input average power is $P = 258.9\,\text{mW}$. The phase of modulation is $\varphi = 0$.

For manufactured DOF which diameter is given by (31) the longitudinal variation of dispersion coefficients β_2 and β_3 can be expressed with the following approximation

$$\beta_2(z) = \langle\beta_2\rangle\,[1 + \beta_{2m}\ \sin(2\pi\ z/z_m + \varphi_m)]\,, \tag{35}$$

$$\beta_3(z) = \langle\beta_3\rangle\,[1 + \beta_{3m}\ \sin(2\pi\ z/z_m + \varphi_m)]\,, \tag{36}$$

where $\langle\beta_2\rangle = -12.76\,\text{ps}^2\text{km}^{-1}$, $\langle\beta_3\rangle = 0.0761\,\text{ps}^3\text{km}^{-1}$, $\beta_{2m} = 0.2$, $\beta_{3m} = 0.095$. The dispersion coefficients (35,36) were evaluated from the measurements of the dispersion of three fibers with the fixed outer diameter: 128 μm, 133 μm and 138 μm. All of three fibers and DOF are manufactured from the same preform.

Nonlinear medium polarization includes the Kerr effect and delayed Raman response $P_{NL}(z,t) = \gamma(z)|A|^2A + \gamma_R(z)QA(z,t)$, where $\gamma(z)$ and $\gamma_R(z)$ are nonlinear coefficients:

$$\gamma(z) = \langle\gamma\rangle\,[1 - \gamma_m\ \sin(2\pi\ z/z_m + \varphi_m)]\,, \tag{37}$$

$$\gamma_R(z) = \langle\gamma_R\rangle\,[1 - \gamma_m\ \sin(2\pi\ z/z_m + \varphi_m)]\,, \tag{38}$$

$\langle\gamma\rangle = 8.2\,\text{W}^{-1}\text{km}^{-1}$ and $\langle\gamma_R\rangle = 1.8\,\text{W}^{-1}\text{km}^{-1}$, $\gamma_m = 0.028$. These coefficients are obtained by calculating of effective area of fundamental mode.

The equation (10) was solved using standard split-step Fourier algorithm (see section 2.2). Simulations were carried out with hyperbolic secant input pulses. In simulations, we characterize the input pulses by the soliton number (order) N. The number of pulses that arise due to the splitting of high-order soliton is determined primarily by N (Bauer et al., 1995; Hasegava et al., 1991; Malomed, 2006).

The pulse splitting is most efficient in resonant regime when the modulation period z_m is equal to the soliton period $z_0 = 0.16\pi|\langle\beta_2\rangle|^{-1}T^2_{\text{FWHM}}$ (Hasegava et al., 1991; Tai et al., 1988). For initial pulse width $T_{\text{FWHM}} = 2.05\,\text{ps}$ (Fig.10) the soliton period $z_0 = 0.166\,\text{km}$ is close to the modulation period $z_m = 0.160\,\text{km}$. For $\varphi_m = \pi$ only one modulation period of DOF is necessary for the soliton fission (Fig.10(a)). After propagation of 0.8 km of DOF the temporal separation between resulting pulses become $T = 14\,\text{ps}$. The same value was obtained in experiment (Fig.7(c)). For $\varphi_m = 0$ the soliton fission arises after propagation of 0.6 km in DOF

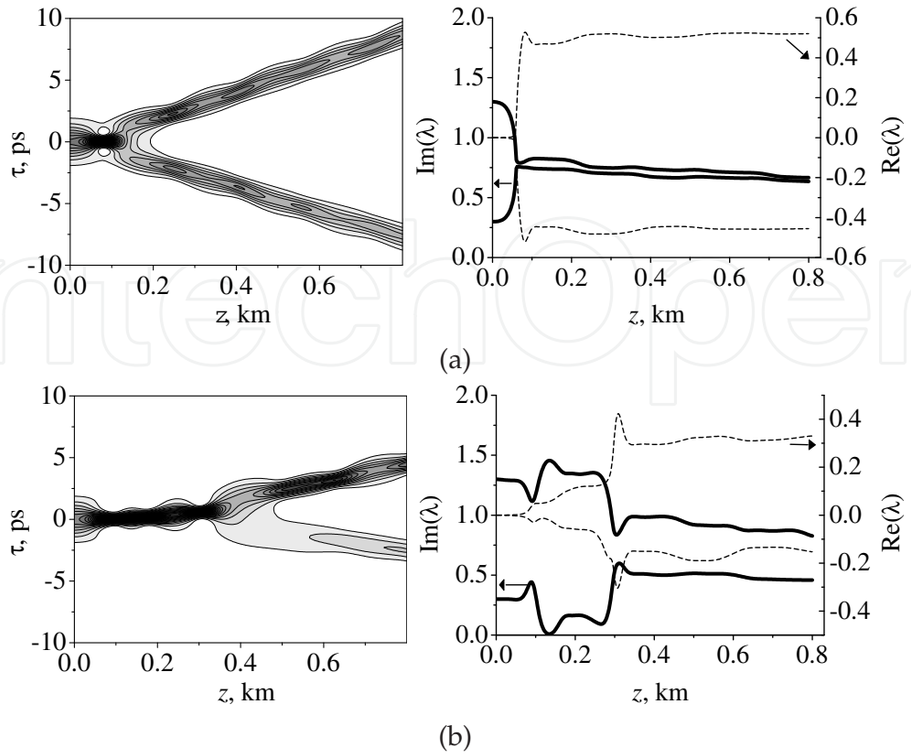

Fig. 10. Numerical simulation of the pulse evolution in DOF. Width of initial pulse is $T_{\text{FWHM}} = 2.05\,\text{ps}$, The pulse has soliton order $N = 1.8$. (a) $\varphi = \pi$. (b) $\varphi = 0$.

(Fig.10(b)). The temporal separation between output pulses is $T = 6.2\,\text{ps}$ that is agree well with experiment (Fig.7(d)).

For the initial pulse width $T_{\text{FWHM}} = 1.75\,\text{ps}$ the soliton period is $z_0 = 0.126\,\text{km}$. This value does not obey the resonant condition $z_0 = z_m$. However for input pulse width $T_{\text{FWHM}} = 1.75\,\text{ps}$ the temporal separation between pulses (Fig.7(a)) is higher than the same for resonant conditions $(T_{\text{FWHM}} = 2.05\,\text{ps},\ z_0 = 0.166\,\text{km} \simeq z_m)$ (Fig.7(c)). Experimental observation is in agreement with calculations. Numerical simulations show that such effect arises due to the simultaneous action of the periodical modulation of the fiber dispersion and stimulated Raman scattering. The frequency red shift due to the Raman scattering is inversely proportional to the fourth power of the pulse width (Tai et al., 1988). As result the change of the pulse group velocity and correspondent temporal separation between pulses will be higher for the shorter pulse width $(T_{\text{FWHM}} = 1.75\,\text{ps})$.

The input soliton decays into pulses with different peak intensities (Fig.10). Such asymmetry arises due to stimulated Raman scattering. For $\varphi_m = \pi$ (Fig.10(a)) the ratio of the peak of low-intensity pulse to the peak of high-intensity pulse is $I_{12} = 0.9$. For $\varphi_m = 0$ (Fig.10(b)) we obtain $I_{12} = 0.21$. Numerical calculations confirm our conclusions (Section 3.1) that the case $\varphi_m = \pi$ is preferable for the symmetrical splitting of input pulse. Note that without stimulated Raman scattering and third-order dispersion term the pulse with $N = 1.8$ does not split (see fig. 5).

The pulses become propagating with different group velocities (Fig.10) due to the shift of the carrier frequency. For the modulation phase $\varphi_m = \pi$ instantaneous frequency shift

of output pulses is shown in Fig.11(a). The first pulse has blue shifted carrier frequency $(\nu_0 - \langle\nu\rangle_1) = -0.105$ THz while for the second pulse the frequency is red shifted $(\nu_0 - \langle\nu\rangle_2) = 0.120$ THz, where $\langle\nu\rangle_{1,2}$ are mean-weighted carrier frequencies of the first and second pulses correspondingly. Pulses are separated well in time domain. This allows to calculate their spectra separately (Fig.11(b)). The first pulse has the central wavelength $\lambda_1 = 1549.60$ nm while the second has $\lambda_2 = 1551.48$ nm. The difference $(\lambda_2 - \lambda_1) = 1.88$ nm is large enough to process the pulses in frequency domain separately using narrow-bandwidth fiber Bragg grating (Othonos et al., 1999), liquid crystal modulator array (Weiner, 1995) or arrayed waveguide grating (Oda et al., 2006), for example. To simulate effect of spectral filtering on the pulses (Fig.11(a,b)) the field after stopband filters $f_+(\omega)$ and $f_-(\omega)$ (39) was calculated.

$$f_\pm(\omega) = 1 - \tanh[(1.5 - (\omega - \omega_0 \pm \Delta))/0.08]/2 - \tanh[(1.5 + (\omega - \omega_0 \pm \Delta))/0.08]/2, \quad (39)$$

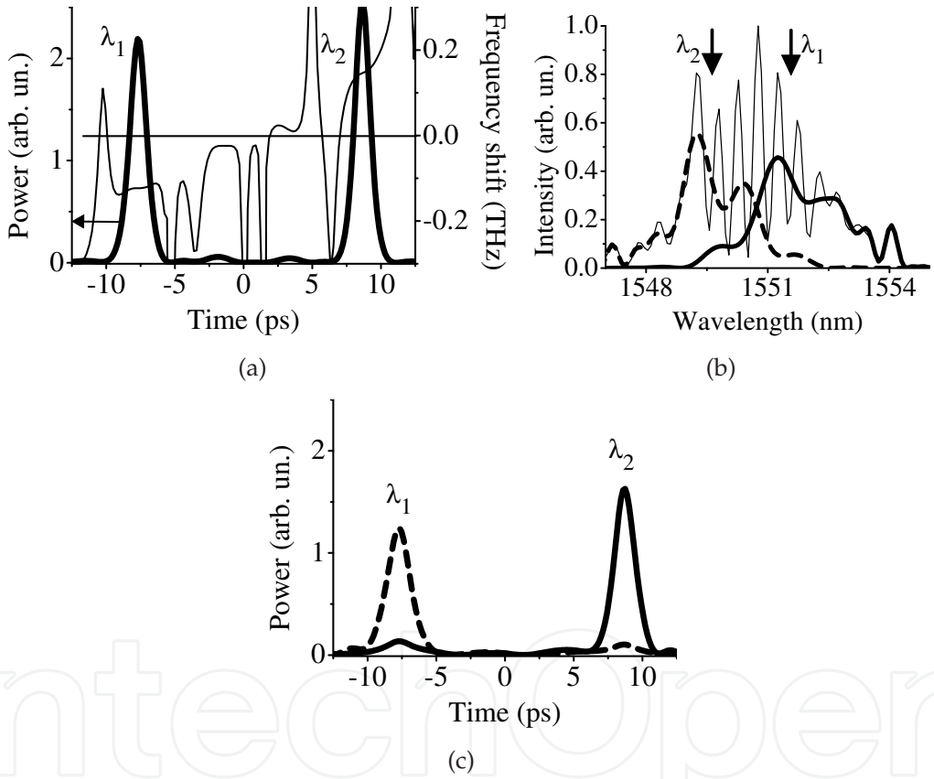

Fig. 11. Simulation of pulse characteristics after propagation in 0.8 km of DOF with $\varphi_m = \pi$. (a) Output intensity (left axis, thick curve) and instantaneous frequency shift (right axis, thin curve). (b) Thick solid curve shows spectrum of the first pulse. Thick dashed curve shows spectrum of the second pulse. Arrows mark central wavelengths λ_1 and λ_2 of the first and second pulses correspondingly. Thin solid curve is the spectrum envelope of the pulse train consists from pair of pulses shown in Fig.(a). The frequency shift was calculated as derivative $\partial \arg(A)/\partial t$. (c) Dashed curve is the pulse after stopband filter f_+ (39) solid curve is the pulse after stopband filter f_-. Simulation parameters are the same as in Fig.10(a)

where $\omega_0 = 2\pi\nu_0$, $\Delta = 1\,\mathrm{ps}^{-1}$. After spectral filtering each half still remains a well defined pulse (Fig.11(c)).
The envelope of the spectrum of the train of output pulse pairs is modulated (Fig.11(b), thin solid curve) due to the interference between pulses. This is in agreement with experimental observations (see Section 3.1).

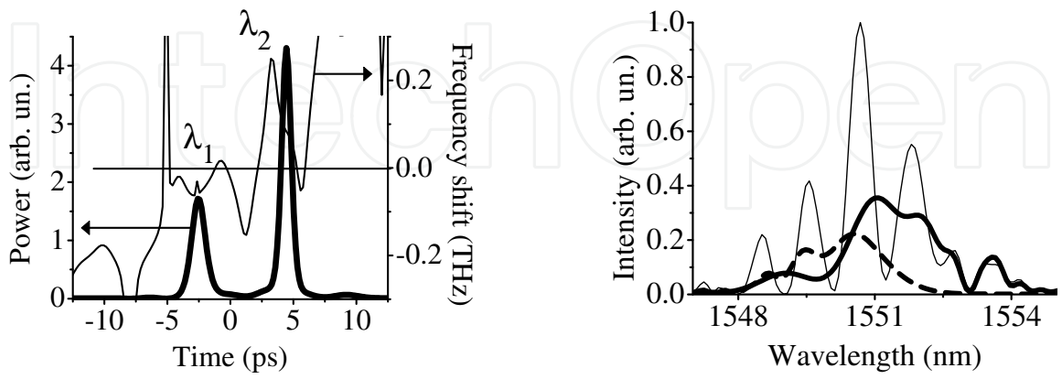

Fig. 12. Simulation of pulse characteristics after propagation in 0.8 km of DOF with $\varphi_m = 0$. (a) Output intensity (left axis, thick curve) and instantaneous frequency shift (right axis, thin curve). (b) Thick solid curve shows spectrum of the first pulse. Thick dashed curve shows spectrum of the second pulse. Thin solid curve is the spectrum envelope of the pulse train consistent from the pulse pairs shown in Fig.(a). Simulation parameters are the same as in Fig.10(b)

For $\varphi_m = 0$ output pulses are shown in Fig.12. The temporal interval between pulses is $T = 5.9\,\mathrm{ps}$ (Fig.12(a)). While for the $\varphi_m = \pi$ the value $T = 13.8\,\mathrm{ps}$ was obtained. The correspondent decrease of the temporal interval between pulse peaks with the change φ_m was observed in experiments (Fig.7). For $\varphi_m = 0$ output pulses are overlapped both in time domain and in frequency domain. Fig.12 demonstrated that deep oscillations of spectrum envelope (thin curve) arise only in region of overlapping of pulse spectra ($1549.0\,\mathrm{nm} < \lambda < 1541.5\,\mathrm{nm}$). The frequency shift for the first pulse is $(\nu_0 - \langle\nu\rangle_1) = -0.041\,\mathrm{THz}$ ($\lambda_1 = 1549.75\,\mathrm{nm}$) while for the second pulse $(\nu_0 - \langle\nu\rangle_2) = 0.093\,\mathrm{THz}$ ($\lambda_2 = 1551.35\,\mathrm{nm}$). The difference between central wavelengths of considered pulses is $(\lambda_2 - \lambda_1) = 1.08\,\mathrm{nm}$. The value $(\lambda_2 - \lambda_1)$ is approximately half the same obtained for $\varphi_m = \pi$ (Fig.11). Overlapping of pulse spectra does not allow to process pulses in frequency domain separately.

4. Pulse propagation in dispersion-decreasing fibers

The fibers with dispersion varying along length have important applications in optical signal processing such as high-quality optical pulse compression, coherent continuum generation, nonlinear dynamic dispersion compensation and other applications (Sysoliatin et al., 2010). This section describes effect of the pulse compression in dispersion-decreasing fibers.
Our experimental setup (Fig.13) includes an actively mode-locked fiber laser operating at 10 GHz as a source of 2.6 ps pulses at central wavelength $\lambda_0 = 1552\,\mathrm{nm}$, high power fiber amplifier, DFDDF (dispersion flattened dispersion decreasing fiber), filter at 1610 nm after the fiber. To analyze the pulse propagation a spectrum analyzer, autocorrelator and power meter

are used. The measurements have been carried out for different levels of EDFA pump current.

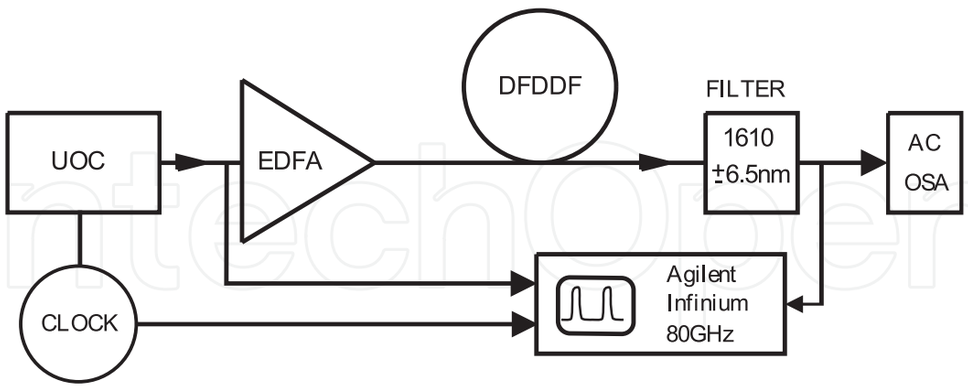

Fig. 13. Experimental setup: Pritel UOC, picosecond pulse source; EDFA, Er-doped fiber amplifier; DFDDF, 42 m length of dispersion flattened dispersion decreasing fiber; AC, autocorrelator "Femtochrome"; OSA, optical spectrum analyzer 'Ando AQ6317"; "Agilent Infinium", sampling scope with 80 GHz bandwidth; "FILTER", WDM filter

The DFDDF fiber has convex dispersion function vs wavelength (Fig.14). In experiments 42 m-length fiber was used. Outer diameter of the fiber decreases from 148 μm to 125 μm, and chromatic dispersion from 10 ps nm^{-1}km^{-1} to -2 ps nm^{-1}km^{-1}. Group velocity dispersion is zero at $z = 40$ m.

Spectrum obtained after propagation of 2.6 ps pulses in DFDDF indicate a red-shifted sideband (fig.15(a)) due to the stimulated Raman scattering (Dianov et al., 1985; Tai et al., 1988). Using commercially available WDM bandpass filter we produce 0.9 ps pulses at 1610 nm. These pulses are synchronized with the input (Fig.15(b)). For a high pulse energies a broadband continuum radiation was observed. However it is essential that the input pulse

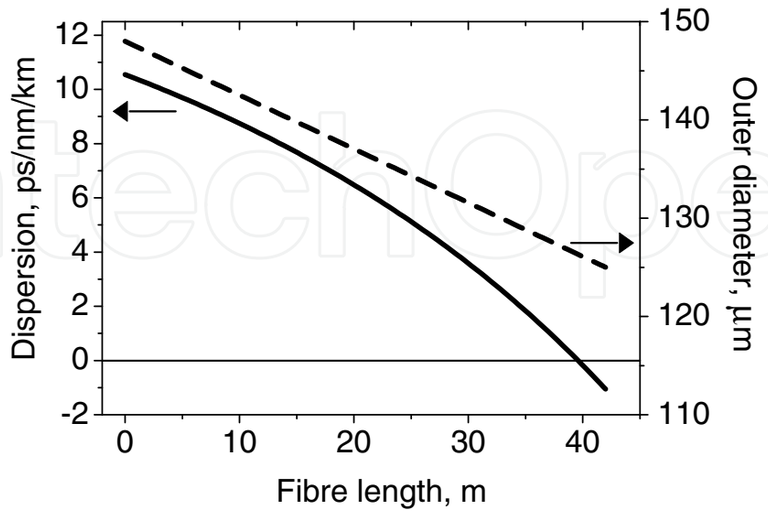

Fig. 14. Dispersion (solid curve) and outer diameter (dashed curve) of DFDDF versus fiber length.

energy should not exceed some critical value to obtain the high quality fully synchronized output pulses at 1610 nm after the filter.

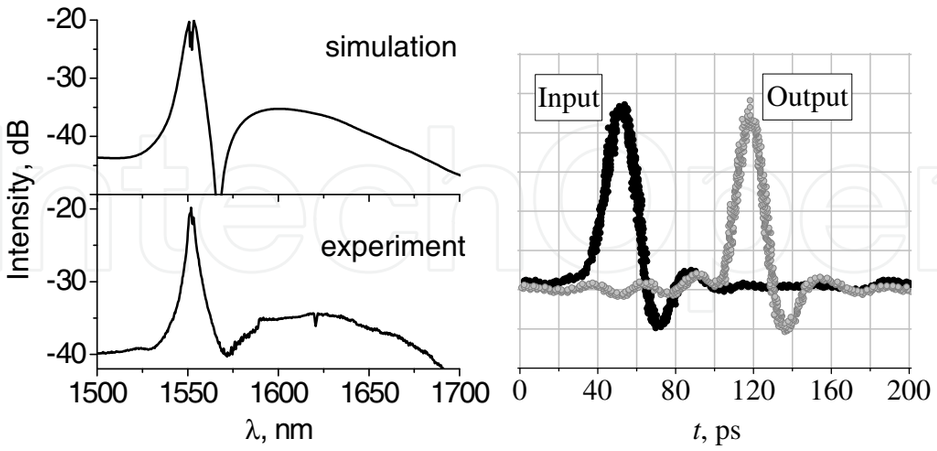

Fig. 15. Output of the DFDDF fiber. (a) Optical spectra obtained by simulation (top) and experimentally (bottom); (b) Sampling scope trace of the pulse at DFDDF input (black color) and output signal of 1610 nm filter (gray color). Input pulse energy is 140 nJ. Pulse repetition rate is 5.37 GHz.

The numerical simulations which model pulse propagation in the DDF are based on the nonlinear Schrödinger equation (10). For manufactured fiber linear absorption coefficient $\alpha = 0.08\,\mathrm{km}^{-1}$, which corresponds to 0.35 dB/km measured loss. Dispersion coefficients $\beta_m(z)$, $(m = 2,3,4,5,6,7)$ take into account longitudinal variation of the fiber dispersion. The approximation $\beta_m(z) = \sum_{k=-2}^{k=3} a_{mk} d(z)^k$ was used. Where $d(z)$ is the DDF outer diameter. Effective area for nonlinear coefficients γ and γ_R (12) is approximated by $A_{\mathrm{eff}} = a_0 + \sum_{j=1,2,3} \left[a_j d^j(z) + b_j d^{-j}(z) \right]$.

Due to the decreasing of the absolute value of the dispersion the initial solitonic pulse is strongly compressed (fig.16(a)). After compression the pulse envelope becomes modulated. As result the generation of Raman red-shifted radiation become efficient. Simulation shows that broadband red-shifted Raman component (Fig.16(b)) appears after the propagation distance $z = 35$ m.

Initial pulse $(z = 0)$ corresponds to four solitons $(N = 4.14)$. There are four solutions λ_j (fig.16(c,d)). The solitonic spectrum (fig.16(c,d)) is plotted up to $z = 40\,\mathrm{m}$. Because for $z > 40\,\mathrm{m}$ GVD is normal. After $z = 15\,\mathrm{m}$ new solutions emerged. (fig.16(d)). The soliton amplitude associated with $Im(\lambda_j)$ (22). While the group velocity associated with $Re(\lambda_j)$. Up to $z = 25\,\mathrm{m}$ all solitons propagate with the same group velocity, because $Re(\lambda_j) = 0$ (fig.16(c)). At $z = 35$ m the pulse is strongly compressed (fig.16(a)) and the soliton splitting appears (fig.16(c,d)). The soliton having maximum amplitude shown by thick solid curve (fig.16(c,d)). This soliton is responsible for generation of broad red-shifted sideband at fiber end (fig.16(b)).

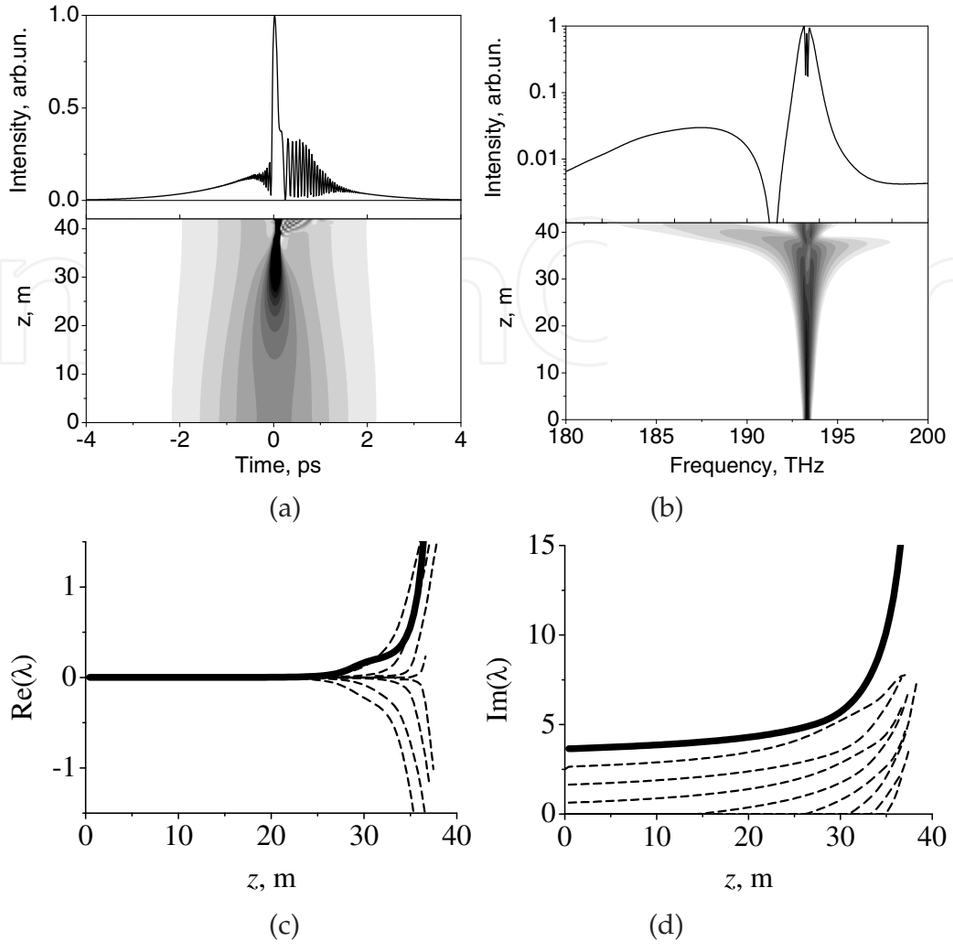

Fig. 16. Simulation of the pulse compression and red-shifted sideband generation. (a) Pulse dynamics. (b) Spectrum dynamics. Top inserts show the the intensity after 42 m propagation in DFDDF. In density plots black color corresponds to higher intensity. (c) Real part of λ_j. (d) Imaginary part of λ_j. Input pulse energy is 140 nJ.

5. Conclusion

The fibers with varying along length chromatic dispersion are of essential interest for nonlinear fiber optics. The fiber parameters variations can be treated as an effective loss or gain. The additional benefit is that the spontaneous emission noise is not amplified in such passive fiber. There are applications of such fibers as the high-quality soliton compression, soliton splitting, stable continuum generation, nonlinear dynamic dispersion compensation in optical network, widely tunable GHz repetition rate all-fiber laser and other.

Using a single-wavelength picosecond pulse laser and dispersion oscillating fiber, the generation of a train of picosecond pulses with alternate carrier frequency was demonstrated. Experimental observations are in agreement with numerical simulations. The model includes the Raman self-frequency shift, third-order dispersion, and nonlinear dispersion as well as the modulation of other fiber parameters. The pulses with different carrier frequencies

are obtained due to the soliton splitting in the fiber with variable dispersion. We focus on the splitting of second-order solitons, because stimulated Raman scattering essentially complicates the dynamics of high-order solitons propagated in manufactured DOF. In this case, high-order soliton splits into a series of low-intensity pulses and a single high-intensity pulse with a large red shift of the carrier frequency. Second-order soliton transmitted through the DOF splits into two pulses with different amplitudes. For various applications, it is preferable to obtain the pulses with the same peak power. For second-order solitons, the difference between the peak powers of output pulses can be reduced by the appropriate choice of the phase of the periodical modulation of the core diameter of the fiber. The split pulses propagate with different group velocities. Transmitting pulses through a fiber with appropriate length, it is possible to achieve the doubling of the repetition rate of input pulse train.

The DOF can be used in principle for the splitting of high-order solitons. The effect of Raman scattering on the soliton splitting depends mainly on the pulse peak power. The peak power of solitons is reduced in a fiber with a small second-order dispersion β_2 . To achieve the splitting of third-or fourth-order solitons without significant effect of Raman scattering, one can use a dispersion oscillating fiber with reduced mean-weighted dispersion. Splitting of high-order solitons will allow increasing the frequency separation of output pulses and building up the efficient multiwavelength optical clock.

Using dispersion decreasing fiber we have demonstrated generation of pulse sideband having large frequency red-shift. The sideband is coherent. It allows to generate picosecond pulses using spectral filtering of this sideband. Such technique was applied to construct L-band tunable GHz repetition rate fiber laser. The novel efficient optical scheme allows to generate high quality 0.9 ps pulses at 1610 nm pulses, fully synchronized with basic clock at multi gigahertz pulse repetition rate.

Numerical simulations described in presented chapter reveal the solitons dynamics. Analysis of solitonic spectra (λ_j) give us a tool to optimize fiber dispersion and nonlinearity for most efficient soliton splitting or pulse compression.

6. Acknowledgement

The authors acknowledge the contribution of Dr. K.V. Reddy to this work.

7. References

Ablowitz, M.; Segur, H. (1981) *Solitons and the Inverse Scattering Transform*, SIAM, Philadelphia

Agrawal, G. P. (2001). *Nonlinear Fiber Optics*, 3-rd edition, Academic Press.

Akhmanov, S. A.; Vysloukh, V. A. & Chirkin, A. S. (1991). *Optics of femtosecond laser pulses*, American Institute of Physics.

Andrianov, A. V.; Muraviev, S. V.; Kim, A. V. & Sysoliatin, A. A. (2007). DDF-Based All-Fiber Optical Source of Femtosecond Pulses Smoothly Tuned in the Telecommunication Range. *Laser Physics*, Vol. 17, 1296-1302

Belenov, E. M.; Nazarkin, A. V. & Prokopovich, I. P. (1992) Dynamics of an intense femtosecond pulse in a Raman-active medium, *JETP Letters,* vol. 55, 218-222

Bauer, R. G. & Melnikov L. A. (1995). Multi-soliton fission and quasi-periodicity in a fiber with a periodically modulated core diameter. *Optics Communications*, Vol. 115, 190-195

Brechet, F.; Marcou, J.; Pagnoux, D. & Roy P. (2000). Complete Analysis of the Characteristics of Propagation into Photonic Crystal Fibers by the Finite Element Method. *Optical Fiber Technology*, Vol. 6, 181-191

Dianov, E. M.; Karasik, A. Ya.; Mamishev, P. V.; Prokhorov, A. M.; Serkin, V. N.; Stelmah, M. F. & Fomichev, A. A. (1985). Stimulated-Raman conversion of multisoliton pulses in quartz optical fibers. *JETP Letters,* Vol. 41, 294-297

Driben, R. & Malomed, B. A. (2000). Split-step solitons in long fiber links, *Optics Communications*, Vol. 185, 439-456

Golovchenko, E. A.; Dianov, E. M.; Prokhorov, A. M. & Serkin, V. N. (1985). Decay of optical solitons. *JETP Letters,* Vol. 42, 87-91

Guo, S. & Albin, S. (2004). Comparative analysis of Bragg fibers. *Optics Express*, Vol. 12, No. 1, 198-207

Hasegawa, A. & Kodama Y. (1991) Guiding center solitons. *Physical Review Letters*, Vol. 66, 161-164

Yu, C. X.; Haus, H. A.; Ippen, E. P.; Wong, W. S. & Sysoliatin, A. A. (2000). Gigahertz-repetition-rate mode-locked fiber laser for continuum generation. *Optics Letters*, Vol. 25, 1418-1420

Inoue, T.; Tobioka, H. & Namiki, S. (2005). Stationary rescaled pulse in alternately concatenated fibers with O(1)-accumulated nonlinear perturbations. *Physical Review E*, vol. 72, 025601(R)

Kivshar, Yu. S. & Agrawal, G. P. (2003). *Optical solitons : from fibers to photonic crystals*, San Diego, CA: Academic Press

Lee, K. & Buck, J. (2003). Wavelength conversion through higher-order soliton splitting initiated by localized channel perturbations. *Journal of Optical Society of America B*, Vol. 20, 514-519

Lourtioz, J. M.; Benisty, H.; Berger, V.; Gerard, J. M.; Maystre, D.; Tchelnokov, A. (2005) *Photonic Crystals. Towards Nanoscale Photonic Devices*, Springer-Verlag, Berlin, Heidelberg

Lægsgaard, J.; Mortensen, N. A. & Bjarklev, A. (2003). Mode areas and field-energy distribution in honeycomb photonic bandgap fibers. *Journal of Optical Society of America B*, Vol. 20, No. 10, 2037-2045

Malomed, B. A. (2006). *Soliton management in periodic systems*, Springer.

Oda, S. & Maruta, A. (2006). Two-bit all-optical analog-to-digital conversion by filtering broadened and split spectrum induced by soliton effect or self-phase modulation in fiber. *IEEE Journal of Selected Topics in Quantum Electronics*, Vol. 12, No. 2, 307-314

Othonos, A. & Kalli, K. (1999). *Fiber Bragg Gratings: Fundamentals and Applications in Telecommunications and Sensing*, Boston, Artech House

Pelusi M. D. & Liu H. F. (1997). Higher order soliton pulse compression in dispersion-decreasing optical fibers. *IEEE Journal of Quantum Electronics*, Vol. 33, 1430-1439

Poli, F.; Cucinotta, A.; Selleri, S. (2007). *Photonic Crystal Fibers. Properties and Applications*, Springer Series in Materials Science, Vol. 102

Sears, S; Soljacic, M.; Segev, M.; Krylov, D. & Bergman, K. (2000). Cantor set fractals from solitons. *Physical Review Letters,* Vol. 84, 1902-1905

Smith, N. J.; Knox, F. M.; Doran, N. J., Blow, K. J. & Benion, I. (1996). Enhanced power solitons in optical fibers with periodic dispersion management. *Electronics Letters*, Vol. 32, 54-55

Serkin, V. N.; Hasegawa, A. & Belyaeva, T. L. (2007). Nonautonomous Solitons in External Potentials *Physical Review Letters*, Vol. 98, No. 7, 074102

Snyder, A. W. & Love, J. D. (1983) *Optical waveguide theory*, London, Chapman and Hall Ltd.

Sysoliatin, A.; Belanov, A.; Konyukhov, A.; Melnikov, L. & Stasyuk, V. (2008). Generation of Picosecond Pulse Train With Alternate Carrier Frequencies Using Dispersion Oscillating Fiber, *IEEE Journal of Selected Topics in Quantum Electronics*, Vol. 14, 733-738

Sysoliatin, A.; Konyukhov, A.; Melnikov, L. & Stasyuk, V. (2010). Subpicosecond optical pulse processing via fiber dispersion management. *International journal of microwave and optical technology*, Vol. 5, No. 1, 47-51

Tai, K.; Hasegawa, A. & Bekki N. (1988). Fission of optical solitons induced by stimulated Raman effect. *Optics Letters,* Vol. 13, 392-394

Wai, P. K.; Menyuk, C. R.; Lee, Y. C. & Chen, H. H. (1986) Nonlinear pulse propagation in the neighborhood of the zero dispersion wavelength of monomode optical fibers. *Optics Letters,* Vol. 11, 464-466

Washburn, B. R.; Ralph, S. E. & Windeler, R. S. (2002). Ultrashort pulse propagation in air-silica microstructure fiber. *Optics Express*, Vol. 10, No. 13, 575-580

Weiner, A. M. (1995). Femtosecond optical pulse shaping and processing. *Progress in Quantum Electronics*, Vol. 19, 161-137

Yeh, P.; Yariv, A. & Marom, E. (1978). Theory of Bragg fiber. *Journal of Optical Society of America*, Vol. 68, 1196-1201

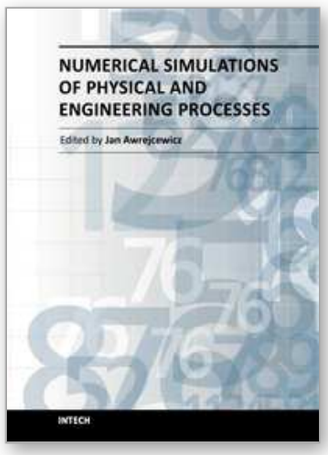

Numerical Simulations of Physical and Engineering Processes

Edited by Prof. Jan Awrejcewicz

ISBN 978-953-307-620-1
Hard cover, 594 pages
Publisher InTech
Published online 26, September, 2011
Published in print edition September, 2011

Numerical Simulations of Physical and Engineering Process is an edited book divided into two parts. Part I devoted to Physical Processes contains 14 chapters, whereas Part II titled Engineering Processes has 13 contributions. The book handles the recent research devoted to numerical simulations of physical and engineering systems. It can be treated as a bridge linking various numerical approaches of two closely inter-related branches of science, i.e. physics and engineering. Since the numerical simulations play a key role in both theoretical and application oriented research, professional reference books are highly needed by pure research scientists, applied mathematicians, engineers as well post-graduate students. In other words, it is expected that the book will serve as an effective tool in training the mentioned groups of researchers and beyond.

How to reference

In order to correctly reference this scholarly work, feel free to copy and paste the following:

Alexej A. Sysoliatin, Andrey I. Konyukhov and Leonid A. Melnikov (2011). Dynamics of Optical Pulses Propagating in Fibers with Variable Dispersion, Numerical Simulations of Physical and Engineering Processes, Prof. Jan Awrejcewicz (Ed.), ISBN: 978-953-307-620-1, InTech, Available from: http://www.intechopen.com/books/numerical-simulations-of-physical-and-engineering-processes/dynamics-of-optical-pulses-propagating-in-fibers-with-variable-dispersion

INTECH
open science | open minds

InTech Europe
University Campus STeP Ri
Slavka Krautzeka 83/A
51000 Rijeka, Croatia
Phone: +385 (51) 770 447
Fax: +385 (51) 686 166
www.intechopen.com

InTech China
Unit 405, Office Block, Hotel Equatorial Shanghai
No.65, Yan An Road (West), Shanghai, 200040, China
中国上海市延安西路65号上海国际贵都大饭店办公楼405单元
Phone: +86-21-62489820
Fax: +86-21-62489821

IntechOpen